Nat Cell Biol. Author manuscript; available in PMC 2012 March 01.

Published in final edited form as:
Nat Cell Biol. ; 13(9): 1029–1039. doi:10.1038/ncb2306.

The tumor suppressor L(3)mbt inhibits neuroepithelial proliferation and acts on insulator elements

Constance Richter[1], **Katarzyna Oktaba**[2], **Jonas Steinmann**[1], **Jürg Müller**[2], and **Juergen A. Knoblich**[1,*]

[1]Institute of Molecular Biotechnology of the Austrian Academy of Science (IMBA), Dr. Bohr-Gasse 3, 1030 Vienna, Austria

[2]European Molecular Biology Laboratory (EMBL), Meyerhofstraße 1, 69117 Heidelberg, Germany

SUMMARY

In *Drosophila,* defects in asymmetric cell division often result in the formation of stem cell derived tumors. Here, we show that very similar terminal brain tumor phenotypes arise through a fundamentally different mechanism. We demonstrate that brain tumors in *l(3)mbt* mutants originate from overproliferation of neuroepithelial cells in the optic lobes caused by de-repression of target genes in the Salvador-Warts-Hippo (SWH) pathway. We use ChIP-seq to identify L(3)mbt binding sites and show that L(3)mbt binds to chromatin insulator elements. Mutating *l(3)mbt* or inhibiting expression of the insulator protein gene *mod(mdg4)* results in upregulation of SWH-pathway reporters. As *l(3)mbt* tumors are rescued by mutations in *bantam* or *yorkie* or by overexpression of *expanded* the deregulation of SWH pathway target genes is an essential step in brain tumor formation. Therefore, very different primary defects result in the formation of brain tumors, which behave quite similarly in their advanced stages.

Development of the *Drosophila* nervous system recapitulates many steps in mammalian neurogenesis. Neurons in the adult fly brain arise from stem cells called neuroblasts which undergo repeated rounds of asymmetric cell division during larval stages [1,2]. After division, one daughter cell remains a neuroblast while the other is called the ganglion mother cell (GMC) and divides just once more into two differentiating neurons. Most larval neuroblasts are inherited from the embryo [3] but the so-called optic lobe neuroblasts (NB) located laterally on each brain lobe (Fig. 1d) pass through a neuroepithelial (NE) stage (Fig. 1e) and are therefore a particularly suitable model for mammalian neurogenesis [4,5]. During early larval stages, the NE cells of the optic lobes (OL) proliferate and separate into the inner (IOA) and outer (OOA) optic anlagen (Fig. 1c, control, cross section) [6,7]. During late larval stages, NE cells switch to a neurogenic mode. On the medial side, they generate optic lobe neuroblasts (OL NBs), which generate the neurons of the medulla, the second optic ganglion [4,8]. OL neurogenesis is controlled by a wave of *lethal of scute* (*l(1)sc*) expression passing through the neuroepithelium from medial to lateral [5]. The activity of the Jak/STAT pathway inhibits neural wave progression and thereby controls neuroblast number. Differentiation of neuroepithelial cells also involves the Notch, Epidermal Growth Factor (EGF) and Salvador-Warts-Hippo (SWH) pathways [9-13].

*To whom correspondence should be addressed: juergen.knoblich@imba.oeaw.ac.at.

Contributions

C.R. conceived and conducted experiments, coordinated the project and wrote the manuscript. K.O. conducted the bioinformatics analysis and conducted experiments. J.S. wrote the peakfinder software and mapped the Solexa reads. J.M. supervised the project. J.K. initiated, designed and supervised the project, conceived experiments and wrote the paper.

Competing financial interests

The authors declare no competing financial interests.

Europe PMC Funders Author Manuscripts

Characterization of *Drosophila* genes identified in brain tumor suppressor screens has demonstrated that defects in neuroblast asymmetric cell division result in the formation of stem cell derived tumors that metastasize and become aneuploid upon transplantation [14,15]. These screens also identified *lethal (3) malignant brain tumor* (*l(3)mbt*) [16,17], a conserved transcriptional regulator [18] that is also required for germ-cell formation in *Drosophila* [19]. L(3)mbt binds to the cell cycle regulators E2F [20] and Rb [21] but the relevance of these interactions is unclear. We show that in *Drosophila*, L(3)mbt regulates target genes of the Salvador-Warts-Hippo (SWH) pathway (Fig. 2i) that are important in proliferation and organ size control [22-24]. The SWH-pathway is regulated by the membrane proteins Expanded (Ex) and Fat, which activate a protein complex containing the kinases Hippo and Warts to phosphorylate the transcriptional co-activator Yorkie [25-27]. Yorkie acts together with the transcription factors Scalloped [28-31] and Homothorax [32] to activate proliferative genes like *Cyclin E* and the microRNA *bantam* (*ban*) [33] and *Drosophila inhibitor of apoptosis 1* (*diap1, thread* in Flybase). Upon phosphorylation, Yorkie is retained in the cytoplasm and its target genes are not activated. In *Drosophila* the main role of the SWH-pathway is to limit proliferation in imaginal discs and its absence leads to tumorous overgrowth [34]. In vertebrates, many homologs of key pathway members are tumor suppressors indicating that this function is conserved [34].

L(3)mbt contains three MBT domains which bind mono- or dimethylated histone tails [21,35]. Biochemical experiments in vertebrates have suggested a role in chromatin compaction [21] but whether this role is conserved is not known. Results published while this paper was under review have shown that germline genes are upregulated in *l(3)mbt* mutant brains and are necessary for tumor formation [36]. Our data indicate that L(3)mbt is bound to insulator sequences, which affect promoter-enhancer interactions and influence transcription [37,38]. In *Drosophila,* the proteins CTCF, CP190, BEAF-32, Su(Hw), Mod(mdg4) and GAF are found at insulator sequences but how these factors act is unknown [38].

Our data show that tumor formation in *l(3)mbt* mutants is initiated by the uncontrolled overproliferation of neuroepithelial cells in the optic lobes due to the upregulation of proliferation control genes normally repressed by the SWH-pathway. L(3)mbt is located at DNA sequences bound by chromatin insulators and we propose that the function of L(3)mbt as a chromatin insulator is essential for repressing SWH target genes and preventing brain tumor formation.

RESULTS

l(3)mbt tumors originate in the optic lobes

l(3)mbt mutants - like *brat* or *lgl* - showed a strong increase in neural stem cells positive for the neuroblast marker Deadpan (Fig. 1a and Supplementary Fig. S1a) resulting in an abnormal enlargement of the brain (Fig. 1a). However, in contrast to *brat* and *lgl* mutants [39-43], the asymmetric segregation of determinants was unaffected (Fig. 1b, Supplementary Fig. S1b and data not shown). Instead, we observed abnormal enlargement of the optic lobes. In wild type brains (Fig. 1c, control) the epithelial monolayer of the OOA forms OL neuroblasts at of its medial edge (Fig. 1d, e). In *l(3)mbt* mutants, the neuroepithelia of both IOA and OOA were massively expanded (Fig. 1c, middle and right panels). Initially, this led to a delay in OL neuroblast formation (Fig. 1c, top view) but later, OL neuroblasts were formed and their number was significantly increased (Fig. 1a, c). Unlike in wild type, neuroblast formation was also seen in the center of the OL epithelium (Fig. 1c, close up). To quantify the epithelial phenotype, we reconstructed optic lobe neuroepithelia (of IOA and OOA) in 3D (see methods). While OL epithelia were on average $1.2\times10^5\mu m^3$ in wild type third instar larvae, their average size was significantly increased to $3\times10^5\mu m^3$ in $l(3)mbt^{76}$ mutants and $8.25\times10^5\mu m^3$ in $l(3)mbt^{76}/Df(3R)D605$ larvae (Fig.

1f). During first larval instar (L1), cell number and mitotic pattern within the OL of *l(3)mbt* mutants were normal and during early second instar (L2 early), the IOA and OOA separated normally (Fig. 1g). However, starting in late second instar (L2 late) the mutant epithelia expanded and started folding. Since tumors did not form in *l(3)mbt* clones and available RNAi lines did not cause OL phenotypes, we generated a small hairpin micro RNA [44] to test cell autonomy of the overproliferation defect. Expression of $l(3)mbt^{shmiR}$ in central brain (CB) neuroblasts resulted in depletion of L(3)mbt protein (Supplementary Fig. S1d) however, this did not cause overproliferation (Supplementary Fig. S1c). In contrast, when expressed in neuroepithelia of the optic lobes $l(3)mbt^{shmiR}$ caused a strong overproliferation in the IOA and OOA (Fig. 1h). Epithelial expansion was also seen in *l(3)mbt* mutant wing imaginal discs (Fig. 3b, c, data not shown and [16]). In most adult wings, this resulted in a significant size increase (Supplementary Fig. S1e, f) but occasionally, very small deformed wings could also be observed. Taken together, these data suggest that overproliferation of neuroepithelial cells during late L2 stages initiates tumor formation in *l(3)mbt* mutants.

Signaling pathways controlling optic lobe proliferation

As staining of *l(3)mbt* mutants for aPKC and Actin did not reveal any change in apical basal polarity (Fig. 2a, b) we used the $GAL4^{C855a}$ driver line to express dominant active, dominant negative and RNAi constructs for the major signaling pathways, epigenetic complexes and epithelial polarity genes (Supplementary Fig. S2e). The $GAL4^{C855a}$ driver is expressed in the IOA and OOA from first to third larval instar and in imaginal disc epithelia (Supplementary Fig. S2a, b). We analyzed epithelial tissue size in the IOA, the OOA and the imaginal discs and estimated the number of OL neuroblasts (Supplementary Fig. S2c, d, e and see methods).

Activation of the epidermal growth factor (EGF) pathway promoted epithelial growth mainly in the IOA (Fig. 2c, S2e). Activation of the Jak/STAT pathway increased epithelial size (Fig. 2d, S2e) [5] whereas deregulation of Dpp or over activation of FGF pathways did not cause any visible phenotypes (Fig. 2c, d).

In contrast, inhibition of the SWH-pathway (Fig. 2i) resulted in a phenotype similar to *l(3)mbt* mutants (Fig. 2f, h, Supplementary Fig. S2e; see also [11]). *expanded* (*ex*) RNAi in the optic lobes (Supplementary Fig. S2c) caused epithelial overproliferation similar to what has been described for *ex* mutants [11]. Overexpression of Hippo together with the apoptotic inhibitor *P35*, strongly reduced the size of optic lobe epithelia (Fig. 2e). Upon expression of non-phosphorylatable Yorkie [26,27], the size of neuroepithelia in the IOA and OOA was five to ten fold increased (Fig 2f, g) a phenotype also observed by Reddy et al. (2010) [11]. A similar albeit milder phenotype was observed upon expression of the Yorkie target *ban* (Fig. 2h, S2e). Thus, inhibition of the SWH-pathway or overexpression of its target genes can recapitulate the increased OL proliferation seen in *l(3)mbt* mutants.

L(3)mbt tumor formation involves the SWH-pathway

The SWH-pathway inhibits expression of *diap1, ban*, and – as part of a negative feedback loop – *ex* (Fig. 2i) [45]. To investigate SWH-pathway activity we used a *diap1-GFP4.3* reporter, in which the second transcriptional start site of *diap1* (TSS2) controls GFP expression (see below for a map of the *diap1* locus and Reference [30]). In wild type brains *diap1-GFP4.3* is expressed in the neuroepithelium of the optic lobes during second and early third larval instars but becomes restricted to three small stripes during mid third instar (Fig. 3a). However, in *l(3)mbt* mutants, *diap1-GFP4.3* remained expressed throughout the overgrowing neuroepithelium (Fig. 3b, note that the high GFP expression in the control is in lamina cells). Moreover, in wing imaginal discs, *diap1-GFP4.3* was upregulated in the entire wing pouch in *l(3)mbt* mutants (Fig. 3b). The *ex-lacZ* reporter was only moderately

expressed in wild type epithelia of the OOA but was upregulated in *l(3)mbt* mutants (Fig. 3c). A similar upregulation was seen in the wing imaginal disc (Fig. 3c). To test *ban*-miRNA activity we used a negative GFP-sensor carrying multiple *ban* binding sites [46]. When *ban* is active this GFP-sensor is downregulated. In control optic lobes the *ban-GFP*-sensor was not detectable indicating strong *ban* expression. The limited dynamic range of the *ban*-GFP-sensor did not allow us to detect further *ban* upregulation in the optic lobes (data not shown). In *l(3)mbt* mutant wing discs, however, GFP was almost completely lost indicating a strong increase in *ban* activity (Fig. 3d). Thus, *l(3)mbt* inhibits the expression of SWH target genes. These effects were cell autonomous and not a consequence of tumor formation since expression of $l(3)mbt^{shmiR}$ in the posterior compartment of the wing disc using $GAL4^{en}$ (*engrailed-GAL4*) increased expression of *ban* (Fig. 3f), *diap1-GFP4.3* (Fig. 3e) and *ex-lacZ* (Fig. 3g) only in this compartment.

To test whether the SWH-pathway is important for tumor formation in *l(3)mbt* mutants, we investigated genetic interactions. In *l(3)mbt* and *ban* double mutants, neuroepithelial size was significantly reduced and tumors did not form (Fig. 4a, compare Supplementary Fig. S4a). Neuroepithelial size was reduced from $4.5\times10^5\mu m^3$ in $ban^1/+; l(3)mbt^{76}$ to less than $1\times10^5\mu m^3$ in $ban^1; l(3)mbt^{76}$ larvae at the same developmental stage (Fig. 4b). Overexpression of Expanded (Ex) rescued the overproliferation in $l(3)mbt^{76}$ mutants (Fig. 4c, d; OL neuroepithelial size $3.3\times10^5\mu m^3$ in $l(3)mbt^{76}$, $1.8\times10^5\mu m^3$ in $GAL4^{C855a}>UAS\text{-}Ex, l(3)mbt/+$ or in $GAL4^{C855a}>UAS\text{-}Ex, l(3)mbt^{76}$). Finally, tumor size in *l(3)mbt* mutants was reduced by removing one copy of *yorkie* (Fig. 4e and Supplementary Fig. S4b, c, d; OL neuroepithelial size $3\times10^5\mu m^3$ in $l(3)mbt^{76/E2}$ and $2.2\times10^5\mu m^3$ in $l(3)mbt^{76}/l(3)mbt^{E2}; yki/+$). Thus the SWH-pathway and its target genes are important for tumor formation in *l(3)mbt* mutants.

L(3)mbt is a nuclear protein

The SWH-pathway regulates gene expression by excluding Yorkie from the nucleus [26,27]. Surprisingly, neither the subcellular localization of Yorkie (Supplementary Fig. S3b and data not shown) nor the expression of the associated transcription factor Scalloped [28-31] (Supplementary Fig. S3a) were changed in OL epithelia or wing discs of *l(3)mbt* mutants, indicating that L(3)mbt does not influence SWH signaling activity.

To analyze the subcellular localization of L(3)mbt we generated a specific antibody (Fig. 5a). In *Drosophila* embryos and in larvae, L(3)mbt was nuclear in interphase and dispersed in the cytoplasm during mitosis (Fig. 5a and data not shown). This staining was specific since it was lost from *l(3)mbt* mutant larvae (data not shown and Western Blot analysis in Supplementary Fig. S5c) and upon $l(3)mbt^{shmiR}$ expression (Supplementary Fig. S1d and Fig. 3e, f, g). The localization was confirmed in flies expressing functional *RFP-L(3)mbt* or *GFP-L(3)mbt* fusions (see also Supplementary Fig. S5a, b). Live imaging of larval neuroblasts expressing *RFP-L(3)mbt* revealed that the protein accumulates in nuclear dots in interphase cells (Fig. 5b). When expressed in salivary glands, L(3)mbt localized to multiple bands on polytene chromosomes that were often characterized by reduced DAPI staining (Fig. 5c). Thus, L(3)mbt is a nuclear protein that most likely exerts its function by associating with chromatin.

L(3)mbt binds to SWH-pathway target loci

To test chromatin binding we performed chromatin immunoprecipitation (ChIP) followed by quantitative PCR analysis from third instar larval brains and imaginal discs (see methods). *diap1* can be transcribed from three promoters, TSS1, TSS2 and TSS3 [28,30]. L(3)mbt bound moderately to TSS2 and strongly to TSS1 (Fig. 6a). Consistent with this, *diap1-GFP5.1* (contains TSS1) was expressed in OL neuroblasts and neurons and strongly upregulated in

l(3)mbt mutants (Fig. 6b). This is surprising because previous reports concluded that TSS1 is not expressed in wing or eye imaginal discs [28,30]. For TSS3, we detected weak binding of L(3)mbt, however, the relevance of this interaction is unclear (Fig. 6a). L(3)mbt did not bind to the bxd Polycomb response element (PRE) in the *Ubx* locus (Fig. 6a) [35] but bound to other SWH target genes like *Cyclin E* (Fig. 6a) [47].

To determine binding sites of L(3)mbt on a genome-wide level, we used Solexa-sequencing. Results from two highly correlated independent ChIP experiments (Pearson correlation 0.8835, Supplementary Fig. S6a) showed that L(3)mbt bound close to TSS (Fig. 6c and see methods). We assigned each bound region to the closest gene (see methods) and conducted a biological pathway (KEGG; Fig. 6d) and gene ontology (GO; Supplementary Fig. S6c) analyses of the predicted target genes [48]. As the SWH-pathway is not yet annotated in these databases it was manually added to our analysis. SWH target genes are among the top 10 pathways overrepresented among L(3)mbt bound genes (data not shown). We identified seven out of eleven known and predicted SWH target genes (*ban, CycA, CycB, CycE, E2f, diap1, fj, ex, Mer, wg, Ser*) and found a significant enrichment (p-value 0.025) of these targets among genes bound by L(3)mbt (Fig. 6f, Supplementary Fig. S6e; 3% FDR). Importantly, the functional binding site at TSS1 of the *diap1* locus (Fig. 6a) was confirmed (Fig. 6f). In addition, we found a low occupancy peak at a conserved site 23kb upstream of the *ban* transcription unit (Fig. 6f). Thus, L(3)mbt binds to multiple SWH target genes.

In our KEGG analysis we also found enrichment for Jak/STAT signaling genes (Fig. 6d and Supplementary Fig. S6e). Jak/STAT signaling previously has been shown to regulate optic lobe neuroepithelial growth [5]. Indeed, the *10xSTAT92E-GFP* sensor was significantly upregulated in both OL neuroepithelia and wing discs of *l(3)mbt* mutants [49] (Fig. 6e). Finally, we found “oocyte maturation” among the top 20 processes enriched in the KEGG and GO analysis (data not shown and Supplementary Fig. S6c). L(3)mbt bound close to the TSS of *vasa* (*vas*), *bag of marbles* (*bam*) and *benign gonial cell neoplasm* (*bgcn*) (Fig. 6h), which may explain the defects in germ cell formation in *l(3)mbt* mutants [19,50].

Microarray analysis of various *Drosophila* brain tumors has identified a set of genes that are specifically deregulated in *l(3)mbt* mutants and are termed L(3)mbt signature (MBTS) genes [36]. 63% of these MBTS genes and 85% of the MBTS genes with a described germline function had L(3)mbt bound within the next +/−2kb (Fig. 6g, Supplementary Fig. S6d), suggesting that the identified L(3)mbt bound regions have in vivo relevance.

L(3)mbt binds to insulator elements

To analyze L(3)mbt binding specificity, we searched for DNA motifs enriched among L(3)mbt binding sites. Among seven DNA consensus motifs, four matched the consensus for the chromatin insulators CP190, BEAF-32, CTCF and Su(Hw) (Fig. 7a) [51-54] whereas, three did not match any known consensus motif (Supplementary Fig. S7a). Using published ChIP-chip data [51] we determined the overlap in binding sites (Fig. 7b). We found a strong overlap of L(3)mbt binding sites with class I chromatin insulators CP190, BEAF-32 and CTCF (Fig. 7b) whereas the overlap with the class II insulator protein Su(Hw) is smaller.

The best-studied locus for insulator proteins is the Hox gene cluster of the Bithorax complex (BX-C) [37,55]. Remarkably, L(3)mbt binding sites within this locus correlated strongly with CP190 and CTCF but less with Su(Hw) (Fig. 7c). To test whether L(3)mbt binding sites in the Hox-cluster are functional, we analyzed the expression of the homeotic gene *Abdominal-B* (*Abd-B*). *CTCF* mutants show a characteristic downregulation of Abd-B at the posterior end of the larval ventral nerve cord (VNC) [55]. We found a significant reduction of Abd-B in *l(3)mbt* mutant larval CNS (Fig. 7d) that closely resembled the change seen in *CTCF*

mutants. Notably, a strong correlation between L(3)mbt and chromatin insulator binding was also observed at the SWH target genes *ban* and *diap1* (Supplementary Fig. S7b, c).

Since we did not observe any deregulation of the *diap1-GFP4.3* reporter upon RNAi mediated knockdown of CTCF, CP190, BEAF-32 and Su(Hw), we tested the insulator protein Mod(mdg4) that binds to CP190 and Su(Hw) but not directly to DNA [56,57]. Upon RNAi mediated knockdown of *mod(mdg4)* bantam-sensor-GFP was strongly downregulated (Fig. 7e, indicating an increase in bantam activity) whereas the *diap1-GFP4.3* reporter was only mildly upregulated (data not shown). Thus, insulator protein function is necessary to control SWH target gene expression.

DISCUSSION

A new mechanism for tumor formation in *Drosophila*

brat, lgl and *dlg* were identified as *Drosophila* brain tumor suppressors. In all cases, defects in asymmetric cell division cause a huge expansion of the neuroblast pool [39-42,58,59]. In *l(3)mbt* mutants, however, the neuroblast pool is expanded because an upregulation of SWH target genes results in a massive expansion of neuroepithelial tissue. Why those neuroblasts proliferate indefinitely upon transplantation [15] is currently not understood for any of those mutants.

While the SWH-pathway is essential for tumorigenesis in *l(3)mbt* mutants, its overactivation can not recapitulate the neuroblast tumor phenotype seen in *l(3)mbt* mutants (this study and Reference [11]). Similar to the multifactorial origin of mammalian tumors, therefore, the combined deregulation of several signaling pathways could be required. The Notch pathway could be involved as it regulates the formation of OL neuroblasts from neuroepithelia [10,12,13] and Notch pathway genes are bound by L(3)mbt (Table S1 and data not shown). We also observe increased activity of the Jak/STAT pathway, a major regulator of OL development [5]. Finally, the deregulation of germline genes in *l(3)mbt* mutants that has been described while this manuscript was under review [36] could provide another exciting explanation.

L(3)mbt acts on insulator elements

Our results indicate that L(3)mbt acts on insulator elements, which isolate promoters from the activity of nearby enhancers acting on other genes [37,38]. Our analysis showed that L(3)mbt binding sites overlap with CP190, CTCF and BEAF-32, placing the protein into what has been called the class I of chromatin insulators [51].

The identification of a DNA consensus motif for a histone binding protein like L(3)mbt is highly unexpected as insulators are typically nucleosome free [51]. Currently, the activity of these important transcriptional regulators could be explained in several ways [37,38]. Either, they form physical barriers blocking the interaction between enhancers and promoters. Alternatively, they mimic promoters and compete with endogenous promoters for enhancer interaction. Finally, they could interact with each other or nuclear structures to form loop domains that regulate transcriptional activity. Our data suggests another model in which insulators interact with histones on nearby nucleosomes and influence the structure of higher order chromatin. Importantly, in the regions flanking CTCF binding sites nucleosomes are enriched for histones that are mono- and di-methylated on H3K4 or mono-methylated on H3K9 or H4K20 [60], the variants to which MBT domains can bind *in vitro* [18,21,35,61]. As the human L(3)mbt homolog L3MBTL1 was shown to compact nucleosome arrays in vitro [21], a model becomes feasible in which simultaneous binding to insulators and the surrounding nucleosomes reduces flexibility and thereby restricts the ability of nearby enhancers to interact with promoters on the other side of the insulator. However, our data could equally

well be worked into the other prevalent models for insulator activity. Since L(3)mbt is currently the only chromatin insulator besides CTCF that is conserved in vertebrates, analysis of its homologs will certainly allow to distinguish between those possibilities.

A conserved role for L(3)mbt

OL development resembles vertebrate neurogenesis [4]. Both processes consist of an initial epithelial expansion phase followed by neurogenesis through a series of asymmetric divisions [62]. Together with previous findings [11], our data demonstrate that *l(3)mbt* and the SWH-pathway are crucial regulators of the initial neuroepithelial proliferation phase. Interestingly, the SWH-pathway has been implicated in regulating neural progenitors in the chicken embryo [63] and it will be exciting to test the role of mammalian L(3)mbt in this process. It is remarkable that YAP is upregulated [64] and L3MBTL3 is deleted in a subset of human medulloblastomas [65]. Medulloblastoma is the leading cause of childhood cancer death and investigating the role of the SWH-pathway might contribute to the progress in fighting this disastrous disease.

Supplementary Material

Refer to Web version on PubMed Central for supplementary material.

Acknowledgments

We wish to thank I. Reichardt, N. Corsini, A. Fischer and C. Jueschke for comments on the manuscript; R. Neumueller and all former and present members of the Knoblich laboratory, as well as Wu Wei, Charles Girardot and Julien Gagneur for discussions; R. Lehmann, D. Pan, L. Zhang, N. Tapon, B. Thompson, G. Halder, G.H. Baeg, M. Labrador, the Flytrap Yale, the Bloomington *Drosophila* Stock Center, the Vienna *Drosophila* RNAi Center (VDRC) and the Developmental Studies Hybridoma Bank (DSHB) for flystocks, antibodies and constructs; P. Serrano Drozdowskyj and M. Novatchkova for bio-informatic support; M. Madalinski for affinity purification; E. Kleiner for technical assistance; K. Aumayr, P. Pasierbek and G. Schmauss for bio-optics support; S. Farina Lopez, S. Wculek and C. Valenta for fly work support. Work in J.A.K.'s laboratory is supported by the Austrian Academy of Sciences, the Austrian Science Fund (FWF) and the EU FP7 network EuroSystem.

Appendix

Methods

Drosophila Strains and Constructs

The *l(3)mbt* alleles used in this study were: $l(3)mbt^{ts1}$, $l(3)mbt^{E2}$ [16,17], $l(3)mbt^{76}$ [19] (original stock contained suppressive second site mutation, chromosome was cleaned during recombination to new FRT82B). All experiments and controls with *l(3)mbt* mutants were conducted at 29°C except if noted otherwise. Other mutant fly strains were: ex^{e1} [66]; yki^{B5} [25]; ban^{delta1} [67]; *Df(3R)D605* (Bloomington). The SWH and Jak/STAT pathway reporter lines were: ex^{697} (*ex-lacZ*) (gift from N.Tapon) [66]; *diap1-GFP4.3* and *diap1-GFP5.1* [30]; *ban-sensor-GFP* [46]; $Sd\text{-}GFPtrap^{CA07575}$ [68]; *10xStat92E-GFP* [49]. See below for complete list of all fly strains.

UAS-constructs for L(3)mbt and Yki were cloned using the Gateway System (Invitrogen). *l(3)mbt* was PCR-amplified from DGRC cDNA clone pB SK LD05287 and *yki* was cloned from mixed stage cDNA. $L(3)mbt^{shmiR}$ was cloned according to Haley et al. (2008) [44]. All experiments with $l(3)mbt^{shmiR}$ were conducted at 32°C except if noted otherwise (over proliferation phenotype in optic lobe neuroepithelia is observed only at 32°C). The following driver lines were used: $GAL4^{1407}$ (*insc-Gal4*) [69] and $GAL4^{C855a}$ [70], $GAL4^{c253}$, $GAL4^{en}$ (all Bloomington Stock Center). All other UAS lines are listed below.

For the candidate screen UAS constructs were crossed to GAL4C^{855a} at 29°C. Phenotypes were determined from z-stacks of stained brains from wandering third instar larvae and scored manually on a scale from −10 to +10 (0 = wild type optic anlagen size; +10 = *l(3)mbt76* mutant optic anlagen; −10 = strong underproliferation).

Image acquisition and live imaging

Images were acquired on a Zeiss LSM510 Meta confocal microscope using 25x (zoom 0.7x for imaginal discs and zoom 1x for brains) or 60x oil immersion objectives (zoom 3x for polytene chromosomes). For live imaging, larval brains were dissected in PBS, mounted in PBS on a round coverslip and covered with bioFOLIE25 (In Vitro Systems and Services, 96077317). For four-dimensional (4D) z-stacks of 15-20 μm at 0.8-1 μm intervals were acquired at 30sec intervals (40x oil immersion objective). A wet chamber prevented evaporation.

NE tumor volume was quantified using Amira 3D reconstruction software. Z-stacks of 40-80 μm were recorded at 2 μm intervals (25x oil immersion objective at 1x zoom). Optic lobe neuroepithelia were outlined manually (Actin positive; Deadpan negative) in each z-slice and the 3D surface and volume were determined automatically. Significance was calculated by using unpaired t-test with Welch's correction and visualized as aligned dot plot with mean and standard error of the mean (SEM).

Antibodies and Immunohistochemistry

L(3)mbt antibodies were raised in guinea pigs against amino acids 1211 to 1477 of the L(3)mbt protein fused to Maltose Binding Protein (MBP) (affinity purified, IF: 1:200, ChIP: ~5μg (10μl for 250μl chromatin)). Other antibodies were rabbit anti-Miranda (1:200; [42]), rat anti-E-Cadherin (1:100, DCAD2, Developmental Studies Hybridoma Bank, University of Iowa, DSHB), guinea pig anti-Deadpan (1:1000, gift from J. Skeath), goat anti-aPKCzeta (1:200, Santa Cruz Biotechnology), mouse and rabbit anti-phospho histone H3 (1:2000, Cell Signaling), mouse anti-Prospero (1:50, MR1A, DSHB), mouse anti-Lamin (1:50, ADL67.10, DSHB), chicken anti-beta Galactosidase (1:500, Abcam), rabbit anti-Yorkie (1:200, Duojia Pan), rabbit anti-dSfmbt$_{531\text{-}980aa}$ (ChIP: 20μl, [61]), rabbit anti-Mod(mdg4) [71], Alexa Fluor 488 and 568 phalloidin (Invitrogen). All secondary antibodies were generated in donkey and were from Invitrogen.

Immunofluorescence experiments in larval brains and discs were carried out as described [42]. Briefly, brain-disc complexes were dissected in PBS and fixed for 15-20min in 4% PFA in PBS, 0.1% TritonX-100 (1 change of fixative); antibodies were diluted in 10% normal donkey serum in PBS, 0.1% TritonX-100; brains were mounted in Vectashield containing DAPI (Vector Laboratories).

Chromatin preparation and ChIP

Chromatin immunoprecipitation (ChIP) experiments were carried out essentially as described in Oktaba el al. (2008) [72]. A detailed protocol can be found on Nature Protocol exchange (http://www.nature.com/protocolexchange/; doi:10.1038/protex.2011.229). Briefly, 200 wild-type (*Canton S* or *w^{1118}*) third instar larvae were dissected in ice-cold PBS. Carcasses were stored at 4°C in wash B (maximal O/N). Brain-disc tissues were hand dissected in wash B and material of 600-800 brain-disc complexes pooled for one chromatin preparation. Sonication of dissected material was performed in 0.5 ml RIPA buffer in two steps (1st: 2x for 2 min with a tip sonicator (Omni-Ruptor 250 (Omni-International Inc.), microtip, power output: 20, pulser: 60; 2nd: 3x for 10 min in a Covaris machine (Covaris S, maximum all)). This resulted in ~500bp fragments for ~80 % of the chromatin. After

centrifugation (4°C, 20min, 16000g) the soluble chromatin in the supernatant was diluted, aliquoted and quick-frozen in liquid nitrogen prior to storage at −80°C.

For ChIPs, 110 or 250 μl of chromatin were incubated with antibodies (anti-L(3)mbt$_{1211\text{-}1477aa}$ and anti-dSfmbt$_{531\text{-}980aa}$) at 4°C O/N. DNA pellets were re-suspended in 500 μl H2O prior to storage at −20°C (10 μl per qPCR reaction, triplicates). For ChIP-Seq 12 ChIPs were pooled into 30 μl H2O and used for library preparation according to the Illumina ChIP-Seq protocol. Primer sequences are shown below.

ChIP-Seq mapping and data analysis

All uniquely mappable reads from two biological replicates were mapped to the genome (FlyBase 5.27) using Bowtie 0.12.5 [73]. Since our data set contained an unusually high number of reads (73 million reads), we developed new peakfinder software called PyPeak that was optimized for rich data sets. For low-ranking peaks PyPeak was comparable to the commonly used MACS software [74] whereas it was superior in identifying high ranking peaks (Supplementary Fig. S7d). PyPeak used the high number of sequences to refine the identified peaks and often identified two independent binding sites where MACS predicted one wide binding region (data not shown). The false discovery rate (FDR) was estimated as the ratio of the number of peaks called in the control to the number of peaks called for the ChIP data for a given threshold. To define a cut off for “true bound regions” we plotted the calculated false discovery rate (FDR) against the peak score (Fig. S6b). We identified a highly stringent set of 3314 L(3)mbt bound regions at a 0.5% FDR, as well as a larger set of 4572 bound regions at a 3% FDR, including more low occupancy peaks. Analysis of the binding site distribution showed that L(3)mbt bound preferentially between 700bp upstream and 200bp downstream of transcriptional start sites (Fig. 6c). Within this promoter proximal section the most frequent L(3)mbt binding site was at 250bp upstream of the TSS. Remarkably, this “peak” contained two maxima with a distance of approximately 150bp.

All ChIP-Seq datasets have been deposited to the GEO repository (GSE29206). The peak finding software is available under the terms of the GNU General Public License and can be downloaded at http://github.com/steinmann/pypeak. The frequency of peak distances with respect to the closest TSS was computed.

Data analyses were done using the *Drosophila melanogaster* BDGP Release 5 (UCSC dm3) genome assembly and the Flybase 5.26 genome annotation release. ChIP-Seq tracks were visualized with the Integrated Genome Browser (IGB) [75]. As background for all L(3)mbt target gene analyses all annotated *D.melanogaster* genes were used.

We assigned to each of the 3314 and 4572 L(3)mbt bound regions (0.5% FDR and 3% FDR) the gene with closest TSS from the peak summit of the region. Bound regions further than ±5kb from a TSS were left without assigned gene (311of 3314 or 9.3% and 415 of 4572 or 9%). 2730 (0.5% FDR) and 3543 (3% FDR) unique genes were assigned as target genes (table S1). The 2730 (0.5% FDR) target genes were tested for enriched GO slim term annotations (www.geneontology.org) with a hypergeometric distribution test. As the number of tested terms is small, p-values were not adjusted for multiple testing.

The Ontologizer application [76] was adapted to test the 3543 (3 % FDR) target genes for enrichment in KEGG pathways (www.genome.jp/kegg/, Release 53.0) and for enriched Gene Ontology (GO) term annotations (www.geneontology.org (biological process subontology)). The significance (posterior probability) of this enrichment is based on a Bayesian model-based gene set analysis (MGSA) [48].

Motif analysis

De novo motif discovery was performed on 100bp long regions centered on the peak summit of the 3314 L(3)mbt bound regions (0.5% FDR) using RSAT (Oligo-analysis tool, Pattern-assembly tool (occ_sig>2 and maximum substitution 1) and Convert-matrix tool for position weight matrix (PWM) conversions) [77] and MEME (parameters: distribution of zero or one occurrence per sequence model, allowing sites on + and − strands, 6 as minimum and 25 as maximum motif width, and as background model a 2-order Markov model) [78] tools. The background in these and all following analyses consisted of repeat-masked sequences around the TSS (−700 to +200bp) of all annotated *D.melanogaster* genes. The GGTT motif was only found using MEME.

Binding site predictions were generated with the Patser tool [79] using the PWMs. The Patser score cut-offs varied for each motif, from ls2 to ls0. Motif enrichment was computed as the ratio of the observed motif frequency in the 3314 L(3)mbt bound regions (0.5% FDR) and in the background. Significance was assessed using a Fisher's exact test. The fraction of regions with motif was assessed in the ranked 4572 L(3)mbt bound regions (3% FDR) and the number of motifs identified in each of the 3314 L(3)mbt bound regions (0.5% FDR) was counted.

For Venn diagram counts two or more regions that overlap with at least one base were merged and defined as a 'common' region. Overlaps were generated using the 3314 L(3)mbt bound regions (0.5% FDR) and regions bound by insulator-associated proteins CP190 (6648), BEAF-32 (4706), CTCF (2487, overlap CTCF-N and CTCF-C) and Su(Hw) (3258, overlap of Su(Hw)-1 and Su(Hw)-2 [51]).

References

1. Doe CQ. Neural stem cells: balancing self-renewal with differentiation. Development. 2008; 135:1575–1587. [PubMed: 18356248]
2. Neumuller RA, Knoblich JA. Dividing cellular asymmetry: asymmetric cell division and its implications for stem cells and cancer. Genes Dev. 2009; 23:2675–2699. [PubMed: 19952104]
3. Prokop A, Technau GM. The origin of postembryonic neuroblasts in the ventral nerve cord of Drosophila melanogaster. Development. 1991; 111:79–88. [PubMed: 1901786]
4. Egger B, Boone JQ, Stevens NR, Brand AH, Doe CQ. Regulation of spindle orientation and neural stem cell fate in the Drosophila optic lobe. Neural Develop. 2007; 2:1.
5. Yasugi T, Umetsu D, Murakami S, Sato M, Tabata T. Drosophila optic lobe neuroblasts triggered by a wave of proneural gene expression that is negatively regulated by JAK/STAT. Development. 2008; 135:1471–1480. [PubMed: 18339672]
6. Hofbauer A, Campos-Ortega JA. Proliferation pattern and early differentiation of the optic lobes in Drosophila melanogaster. Roux Arch Dev Biol. 1990; 198:264–274.
7. Green P, Hartenstein AY, Hartenstein V. The embryonic development of the Drosophila visual system. Cell Tissue Res. 1993; 273:583–598. [PubMed: 8402833]
8. Toriya M, Tokunaga A, Sawamoto K, Nakao K, Okano H. Distinct functions of human numb isoforms revealed by misexpression in the neural stem cell lineage in the Drosophila larval brain. Dev Neurosci. 2006; 28:142–155. [PubMed: 16508311]
9. Wang W, et al. Notch signaling regulates neuroepithelial stem cell maintenance and neuroblast formation in Drosophila optic lobe development. Dev Biol. 2010; 350:414–428. [PubMed: 21146517]
10. Ngo KT, et al. Concomitant requirement for Notch and Jak/Stat signaling during neuroepithelial differentiation in the Drosophila optic lobe. Dev Biol. 2010; 346:284–295. [PubMed: 20692248]
11. Reddy BV, Rauskolb C, Irvine KD. Influence of fat-hippo and notch signaling on the proliferation and differentiation of Drosophila optic neuroepithelia. Development. 2010; 137:2397–2408. [PubMed: 20570939]

12. Egger B, Gold KS, Brand AH. Notch regulates the switch from symmetric to asymmetric neural stem cell division in the Drosophila optic lobe. Development. 2010; 137:2981–2987. [PubMed: 20685734]
13. Yasugi T, Sugie A, Umetsu D, Tabata T. Coordinated sequential action of EGFR and Notch signaling pathways regulates proneural wave progression in the Drosophila optic lobe. Development. 2010; 137:3193–3203. [PubMed: 20724446]
14. Gateff E. Malignant neoplasms of genetic origin in Drosophila melanogaster. Science. 1978; 200:1448–1459. [PubMed: 96525]
15. Caussinus E, Gonzalez C. Induction of tumor growth by altered stem-cell asymmetric division in Drosophila melanogaster. Nat Genet. 2005; 37:1125–1129. [PubMed: 16142234]
16. Gateff E, Loffler T, Wismar J. A temperature-sensitive brain tumor suppressor mutation of Drosophila melanogaster: developmental studies and molecular localization of the gene. Mech Dev. 1993; 41:15–31. [PubMed: 8507589]
17. Wismar J, et al. The Drosophila melanogaster tumor suppressor gene lethal(3)malignant brain tumor encodes a proline-rich protein with a novel zinc finger. Mech Dev. 1995; 53:141–154. [PubMed: 8555106]
18. Bonasio R, Lecona E, Reinberg D. MBT domain proteins in development and disease. Semin Cell Dev Biol. 2010; 21:221–230. [PubMed: 19778625]
19. Yohn CB, Pusateri L, Barbosa V, Lehmann R. l(3)malignant brain tumor and three novel genes are required for Drosophila germ-cell formation. Genetics. 2003; 165:1889–1900. [PubMed: 14704174]
20. Lewis PW, et al. Identification of a Drosophila Myb-E2F2/RBF transcriptional repressor complex. Genes Dev. 2004; 18:2929–2940. [PubMed: 15545624]
21. Trojer P, et al. L3MBTL1, a histone-methylation-dependent chromatin lock. Cell. 2007; 129:915–928. [PubMed: 17540172]
22. Reddy BV, Irvine KD. The Fat and Warts signaling pathways: new insights into their regulation, mechanism and conservation. Development. 2008; 135:2827–2838. [PubMed: 18697904]
23. Zeng Q, Hong W. The emerging role of the hippo pathway in cell contact inhibition, organ size control, and cancer development in mammals. Cancer Cell. 2008; 13:188–192. [PubMed: 18328423]
24. Saucedo LJ, Edgar BA. Filling out the Hippo pathway. Nat Rev Mol Cell Biol. 2007; 8:613–621. [PubMed: 17622252]
25. Huang J, Wu S, Barrera J, Matthews K, Pan D. The Hippo Signaling Pathway Coordinately Regulates Cell Proliferation and Apoptosis by Inactivating Yorkie, the Drosophila Homolog of YAP. Cell. 2005; 122:421–434. [PubMed: 16096061]
26. Dong J, et al. Elucidation of a universal size-control mechanism in Drosophila and mammals. Cell. 2007; 130:1120–1133. [PubMed: 17889654]
27. Oh H, Irvine KD. In vivo regulation of Yorkie phosphorylation and localization. Development. 2008; 135:1081–1088. [PubMed: 18256197]
28. Wu S, Liu Y, Zheng Y, Dong J, Pan D. The TEAD/TEF family protein Scalloped mediates transcriptional output of the Hippo growth-regulatory pathway. Dev Cell. 2008; 14:388–398. [PubMed: 18258486]
29. Zhao B, et al. TEAD mediates YAP-dependent gene induction and growth control. Genes Dev. 2008; 22:1962–1971. [PubMed: 18579750]
30. Zhang L, et al. The TEAD/TEF family of transcription factor Scalloped mediates Hippo signaling in organ size control. Dev Cell. 2008; 14:377–387. [PubMed: 18258485]
31. Goulev Y, et al. SCALLOPED Interacts with YORKIE, the Nuclear Effector of the Hippo Tumor-Suppressor Pathway in Drosophila. Curr Biol. 2008; 18:435–441. [PubMed: 18313299]
32. Peng HW, Slattery M, Mann RS. Transcription factor choice in the Hippo signaling pathway: homothorax and yorkie regulation of the microRNA bantam in the progenitor domain of the Drosophila eye imaginal disc. Genes Dev. 2009; 23:2307–2319. [PubMed: 19762509]
33. Thompson BJ, Cohen SM. The Hippo pathway regulates the bantam microRNA to control cell proliferation and apoptosis in Drosophila. Cell. 2006; 126:767–774. [PubMed: 16923395]

34. Harvey K, Tapon N. The Salvador-Warts-Hippo pathway - an emerging tumour-suppressor network. Nat Rev Cancer. 2007; 7:182–191. [PubMed: 17318211]
35. Grimm C, et al. Molecular recognition of histone lysine methylation by the Polycomb group repressor dSfmbt. EMBO J. 2009; 28:1965–1977. [PubMed: 19494831]
36. Janic A, Mendizabal L, Llamazares S, Rossell D, Gonzalez C. Ectopic expression of germline genes drives malignant brain tumor growth in Drosophila. Science. 2010; 330:1824–1827. [PubMed: 21205669]
37. Valenzuela L, Kamakaka RT. Chromatin insulators. Annu Rev Genet. 2006; 40:107–138. [PubMed: 16953792]
38. Bushey AM, Dorman ER, Corces VG. Chromatin insulators: regulatory mechanisms and epigenetic inheritance. Mol Cell. 2008; 32:1–9. [PubMed: 18851828]
39. Lee CY, Robinson KJ, Doe CQ. Lgl, Pins and aPKC regulate neuroblast self-renewal versus differentiation. Nature. 2006; 439:594–598. [PubMed: 16357871]
40. Lee CY, Wilkinson BD, Siegrist SE, Wharton RP, Doe CQ. Brat Is a Miranda Cargo Protein that Promotes Neuronal Differentiation and Inhibits Neuroblast Self-Renewal. Dev Cell. 2006; 10:441–449. [PubMed: 16549393]
41. Bello B, Reichert H, Hirth F. The brain tumor gene negatively regulates neural progenitor cell proliferation in the larval central brain of Drosophila. Development. 2006; 133:2639–2648. [PubMed: 16774999]
42. Betschinger J, Mechtler K, Knoblich JA. Asymmetric segregation of the tumor suppressor brat regulates self-renewal in Drosophila neural stem cells. Cell. 2006; 124:1241–1253. [PubMed: 16564014]
43. Bowman SK, et al. The tumor suppressors Brat and Numb regulate transit-amplifying neuroblast lineages in Drosophila. Dev Cell. 2008; 14:535–546. [PubMed: 18342578]
44. Haley B, Hendrix D, Trang V, Levine M. A simplified miRNA-based gene silencing method for Drosophila melanogaster. Dev Biol. 2008; 321:482–490. [PubMed: 18598689]
45. Pan D. Hippo signaling in organ size control. Genes Dev. 2007; 21:886–897. [PubMed: 17437995]
46. Brennecke J, Hipfner DR, Stark A, Russell RB, Cohen SM. bantam Encodes a Developmentally Regulated microRNA that Controls Cell Proliferation and Regulates the Proapoptotic Gene hid in Drosophila. Cell. 2003; 113:25–36. [PubMed: 12679032]
47. Harvey KF, Pfleger CM, Hariharan IK. The Drosophila Mst ortholog, hippo, restricts growth and cell proliferation and promotes apoptosis. Cell. 2003; 114:457–467. [PubMed: 12941274]
48. Bauer S, Gagneur J, Robinson PN. GOing Bayesian: model-based gene set analysis of genome-scale data. Nucleic Acids Res. 2010; 38:3523–3532. [PubMed: 20172960]
49. Bach EA, et al. GFP reporters detect the activation of the Drosophila JAK/STAT pathway in vivo. Gene Expr Patterns. 2007; 7:323–331. [PubMed: 17008134]
50. Gateff E, Miyamoto T. The Tumor Suppressor Gene Lethal (3) Malignant Brain Tumor (l (3) mbt) of Drosophila Melanogaster: Multiple Functions During Development. Oncogenes in cancer diagnosis. 1990; 39:135–141.
51. Negre N, et al. A comprehensive map of insulator elements for the Drosophila genome. PLoS Genet. 2010; 6:e1000814. [PubMed: 20084099]
52. Zhao K, Hart CM, Laemmli UK. Visualization of chromosomal domains with boundary element-associated factor BEAF-32. Cell. 1995; 81:879–889. [PubMed: 7781065]
53. Holohan EE, et al. CTCF genomic binding sites in Drosophila and the organisation of the bithorax complex. PLoS Genet. 2007; 3:e112. [PubMed: 17616980]
54. Adryan B, et al. Genomic mapping of Suppressor of Hairy-wing binding sites in Drosophila. Genome Biol. 2007; 8:R167. [PubMed: 17705839]
55. Mohan M, et al. The Drosophila insulator proteins CTCF and CP190 link enhancer blocking to body patterning. EMBO J. 2007; 26:4203–4214. [PubMed: 17805343]
56. Pai CY, Lei EP, Ghosh D, Corces VG. The centrosomal protein CP190 is a component of the gypsy chromatin insulator. Mol Cell. 2004; 16:737–748. [PubMed: 15574329]

57. Gause M, Morcillo P, Dorsett D. Insulation of enhancer-promoter communication by a gypsy transposon insert in the Drosophila cut gene: cooperation between suppressor of hairy-wing and modifier of mdg4 proteins. Mol Cell Biol. 2001; 21:4807–4817. [PubMed: 11416154]
58. Ohshiro T, Yagami T, Zhang C, Matsuzaki F. Role of cortical tumour-suppressor proteins in asymmetric division of Drosophila neuroblast. Nature. 2000; 408:593–56. [PubMed: 11117747]
59. Peng CY, Manning L, Albertson R, Doe CQ. The tumour-suppressor genes lgl and dlg regulate basal protein targeting in Drosophila neuroblasts. Nature. 2000; 408:596–600. [PubMed: 11117748]
60. Fu Y, Sinha M, Peterson CL, Weng Z. The insulator binding protein CTCF positions 20 nucleosomes around its binding sites across the human genome. PLoS Genet. 2008; 4:e1000138. [PubMed: 18654629]
61. Klymenko T, et al. A Polycomb group protein complex with sequence-specific DNA-binding and selective methyl-lysine-binding activities. Genes Dev. 2006; 20:1110–1122. [PubMed: 16618800]
62. Gotz M, Huttner WB. The cell biology of neurogenesis. Nat Rev Mol Cell Biol. 2005; 6:777–788. [PubMed: 16314867]
63. Cao X, Pfaff SL, Gage FH. YAP regulates neural progenitor cell number via the TEA domain transcription factor. Genes Dev. 2008; 22:3320–3334. [PubMed: 19015275]
64. Fernandez-L A, et al. YAP1 is amplified and up-regulated in hedgehog-associated medulloblastomas and mediates Sonic hedgehog-driven neural precursor proliferation. Genes Dev. 2009; 23:2729–2741. [PubMed: 19952108]
65. Northcott PA, et al. Multiple recurrent genetic events converge on control of histone lysine methylation in medulloblastoma. Nat Genet. 2009; 41:465–472. [PubMed: 19270706]

Europe PMC Funders Author Manuscripts

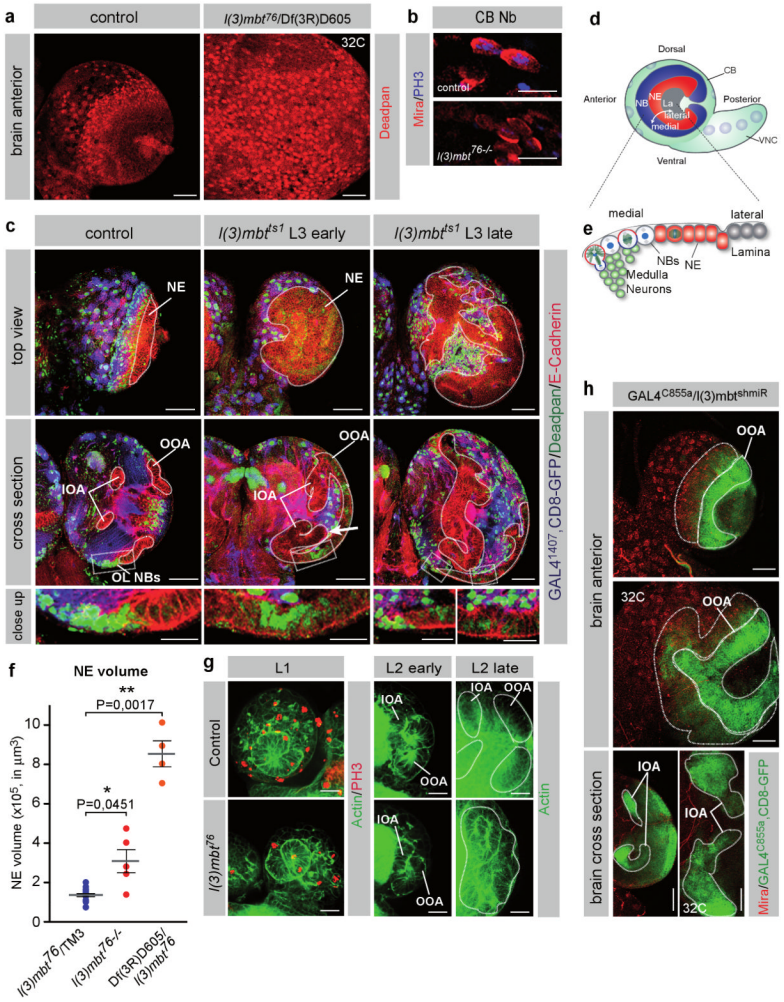

Figure 1. *l(3)mbt* is necessary to prevent tumorous over proliferation of the larval CNS

(**a**) Brains of control and *l(3)mbt*^{76}/Df(3R)D605 larvae raised at 32°C stained for Deadpan (anterior). Scale bars represent 50 μm.

(**b**) Brains of control and *l(3)mbt*^{76} mutant larvae stained for Miranda and PH3 (for overview see Supplementary Fig. S1b). Scale bars represent 20 μm.

(**c**) Brains of control and *l(3)mbt*^{ts1} mutant larvae expressing *GAL4*^{1407}*,CD8-GFP* and stained for Deadpan and E-Cadherin. Upper panels show top views (anterior side) with optic lobe neuroepithelia (NE) outlined. Middle panels show cross section through brain, optic lobe tissues are outlined: neuroepithelia (NE) of inner optic anlagen (IOA), NE of outer optic anlagen (OOA) and optic lobe neuroblasts (OL NBs). White boxes outline close up cross section views that are shown in the lowest panel. White arrow points to folding of IOA. Scale bars represent 50 μm in top rows and 20 μm in bottom row (close up).

(**d**) Schematic drawing of mid-late third instar larval brain (lateral view). Optic lobes consist of outer (OOA) and inner optic anlagen (IOA). Only OOA are shown, which consist of neuroblasts (NB, dark blue), neuroepithelial cells (NE, red) and lamina cells (La, grey). Central brain (CB) and ventral nerve cord (VNC) neuroblasts in light blue (larger circles) and CB neurons in green.

(**e**) Schematic drawing of neurogenesis in outer optic anlagen. Neuroepithelial cells (NE, red) give rise to medulla neuroblasts (NB, blue) and lamina cells (grey). NBs give rise to medulla neurons (green).

(**f**) Quantification of optic lobe neuroepithelial (NE) volume for the following genotypes: *l(3)mbt*^{76}/TM3 (N=16), *l(3)mbt*$^{76-/-}$ (N=5) and Df(3R)D605/*l(3)mbt*^{76} (N=4). N is the number of brain hemispheres quantified. Error bars indicate standard error of the mean (SEM).

(**g**) First and second instar stage optic lobes of control and *l(3)mbt*^{76} mutant brains stained for PH3 (left panel only) and Actin. Note that in late L2 inner and outer optic anlagen (IOA, OOA) are clearly detectable in control brains whereas they are indistinguishable in the *l(3)mbt*^{76} mutants. Scale bars represent 20 μm.

(**h**) Outer optic anlagen (OOA) (upper two panels) and inner optic anlagen (IOA) (bottom panels) of third instar brains expressing *GAL4*^{C855a}*, CD8-GFP, l(3)mbt*^{shmiR} at 29°C (top and bottom left panel) and 32°C (middle and bottom right panel) (see methods) stained for Miranda. Scale bars represent 50 μm.

Europe PMC Funders Author Manuscripts

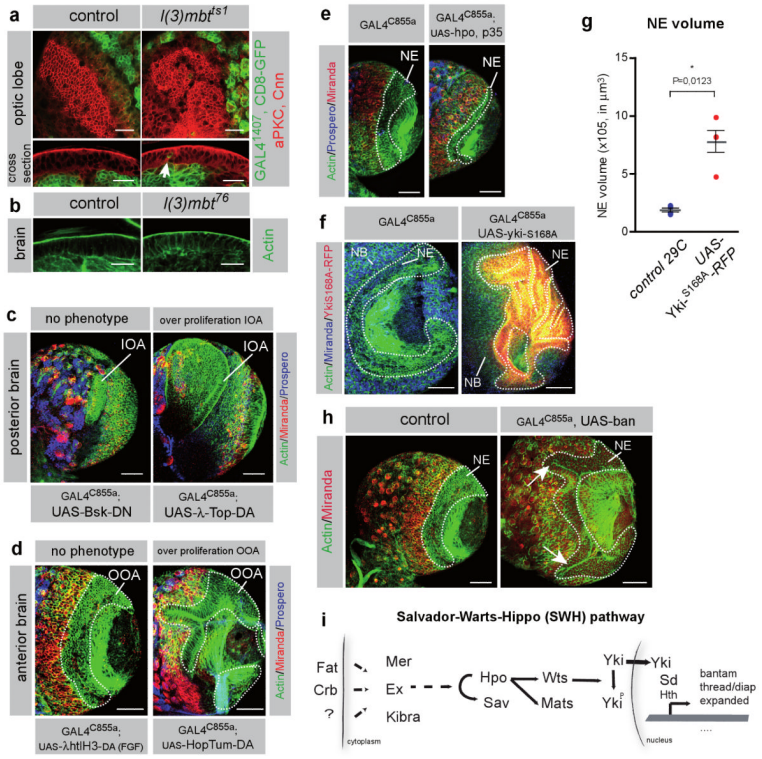

Figure 2. Candidate screen reveals function for SWH-pathway in optic lobe proliferation

(**a**) Optic lobes of control and *l(3)mbt*^{ts1} mutant brains expressing *GAL4*^{1407}*, CD8-GFP* and stained for aPCK and Cnn (same channel, surface and cross section views). Note the mitotic *GAL4*^{1407}*, CD8-GFP* positive cell within the mutant epithelium (white arrow). Scale bars represent 20 μm.

(**b**) Optic lobe epithelium in cross section view of control and *l(3)mbt*^{76} mutant brains stained for Actin. Scale bars represent 20 μm.

(**c**) Larval brains expressing a dominant active (DA) form of Egfr (*λ-Top*) display strong overproliferation of inner optic anlagen (IOA) neuroepithelia whereas a dominant negative (DN) form of Bsk has no phenotype. Brains express *GAL4*^{C855a} and are stained for Actin, Miranda and Prospero. Scale bars represent 50 μm.

(**d**) Larval brains expressing a dominant active (DA) form of Jak (*Hop*^{Tum}) show overproliferation of outer optic anlagen (OOA, outline) whereas a dominant active (DA) form of FGF receptor lambda-Htl-H3 has no phenotype. All brains express *GAL4*^{C855a} and are stained for Actin, Miranda and Prospero. Scale bars represent 50 μm.

(**e**) Larval brains expressing Hpo and anti-apoptotic p35 permanently activate the Salvador-Warts-Hippo (SWH) pathway and show underproliferation of optic lobe neuroepithelia (NE, outlined) whereas control brains show no phenotype. All brains express *GAL4*^{C855a} and are stained for Actin, Miranda and Prospero. Scale bars represent 50 μm.

(**f**) Larval brains expressing dominant active (DA) *Yki*^{S168A}*-RFP* show strong overproliferation of optic lobe neuroepithelia (NE, outlined) but no overproliferation of neuroblasts (NB) whereas control brains show no phenotype. All brains express *GAL4*^{C855a} and are stained for Actin and Miranda. Scale bars represent 50 μm.

(**g**) Quantification of optic lobe neuroepithelial (NE) volume of control (N=11) and *Yki*^{S168A}*-RFP* (N=4) expressing brains. N is the number of brain hemispheres quantified. Error bars indicate SEM.

Europe PMC Funders Author Manuscripts

(**h**) Larval brains expressing *ban* miRNA show overproliferation of optic lobe neuroepithelia (NE, outlined, arrows) whereas control brains show no phenotype. All brains express *GAL4*^{C855a} and are stained for Actin and Miranda. Scale bars represent 50 μm.
(**i**) Schematic drawing of the Salvador-Warts-Hippo (SWH) pathway.

Europe PMC Funders Author Manuscripts

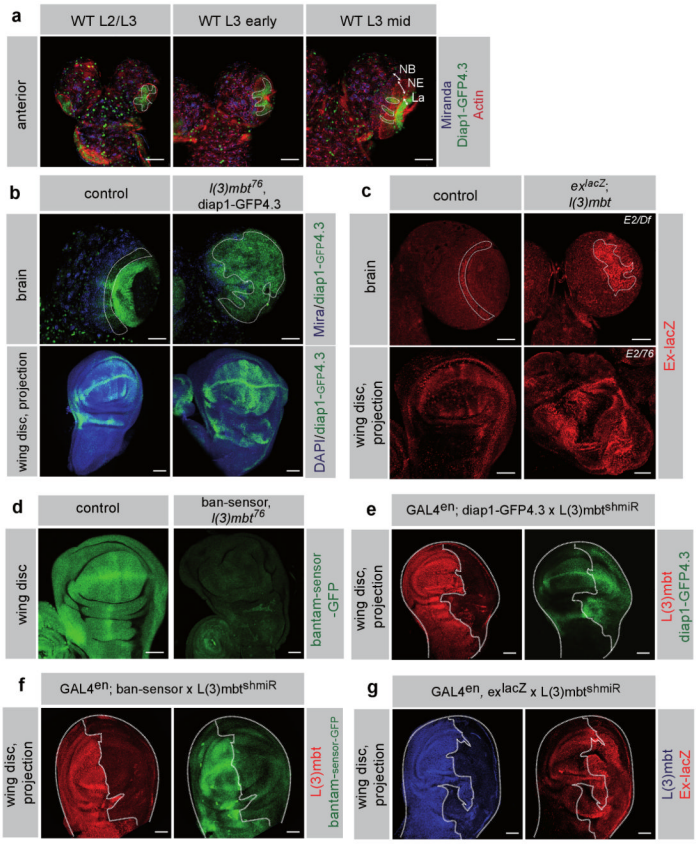

Figure 3. SWH target genes are misregulated in *l(3)mbt* mutants

(**a**) Simulated time course of optic lobe development from second to third larval instar stage in WT brains expressing *diap1-GFP4.3* (outlined) and stained for Miranda and Actin. Note the changing expression pattern of *diap1-GFP4.3* in optic lobes. Optic lobes consist of neuroblasts (NB), neuroepithelial cells (NE) and lamina cells (La). Scale bars represent 50 μm.

(**b**) *diap1-GFP4.3* expressed in control and *l(3)mbt*^{76} mutant brains stained for Miranda (Mira, top panels, optic lobe neuroepithelia are outlined). *diap1-GFP4.3* expressed in control and *l(3)mbt*^{76} mutant wing discs stained for DAPI (bottom panels, maximum intensity projections). Each genotype contains one copy of *diap1-GFP4.3*. Scale bars represent 50 μm.

(**c**) *ex-lacZ* (*ex*^{697}) expressed in control and *l(3)mbt*^{E2}/*Df* mutant brains (top panels) stained for LacZ, optic lobe neuroepithelia are outlined. *ex-lacZ* expressed in control and *l(3)mbt*^{E2}/*Df* mutant wing discs stained for LacZ (bottom panels, maximum intensity projections). Each genotype contains one copy of *ex-lacZ*. Scale bars represent 50 μm.

(**d**) *bantam-Sensor-GFP* expressed in control and *l(3)mbt*^{76} mutant wing discs. Note that *bantam-sensor-GFP* is reduced in *l(3)mbt*^{76} mutants reflecting an increase in *bantam* activity. Each genotype contains one copy of *bantam-sensor-GFP*. Scale bars represent 50 μm.

(**e**) Wing disc expressing *GAL4*^{en}; *diap1-GFP4.3*; *UAS-l(3)mbt*^{shmiR} and stained for L(3)mbt (maximum intensity projection). Scale bars represent 50 μm.

(**f**) Wing disc expressing *GAL4*^{en}; *bantam-sensor-GFP*; *UAS-l(3)mbt*^{shmiR} and stained for L(3)mbt (maximum intensity projection). Scale bars represent 50 μm.

(**g**) Wing disc expressing *GAL4*^{en}; *ex-lacZ*; *UAS-l(3)mbt*^{shmiR} and stained for L(3)mbt and LacZ (maximum intensity projection). Scale bars represent 50 μm.

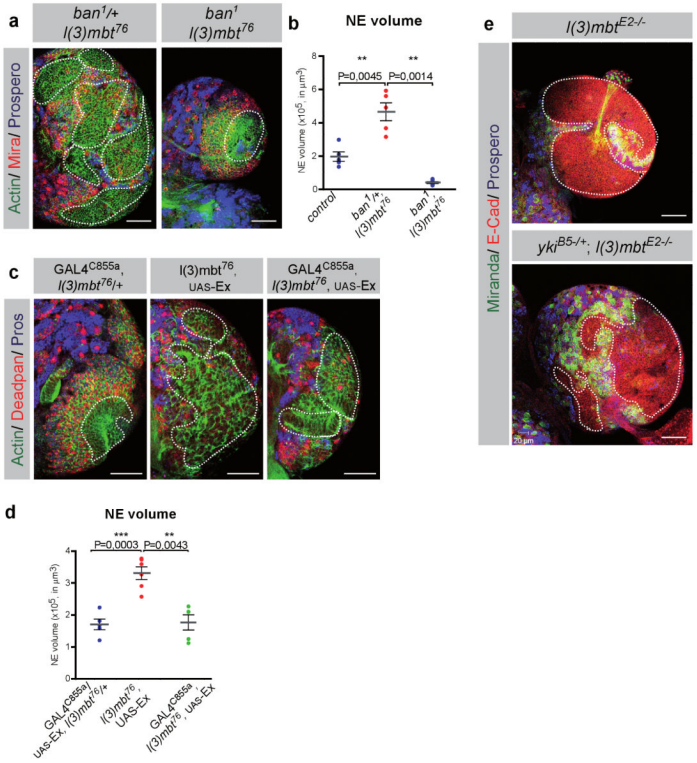

Figure 4. SWH-pathway shows genetic interaction with *l(3)mbt*

(**a**) Genetic interaction of *ban*^{1} and *l(3)mbt*^{76}: *ban*^{1}/+, *l(3)mbt*^{76} mutant brain and *ban*^{1}, *l(3)mbt*^{76} double mutant brain stained for Actin, Miranda and Prospero. Double mutants display the *ban*^{1} phenotype (see also Fig. S4a). Scale bars represent 50 μm.

(**b**) Quantification of optic lobe neuroepithelial (NE) volume of *ban*^{1}, *l(3)mbt*^{76}/TM6 (control) (N=5), *ban*^{1}/+, *l(3)mbt*^{76} (N=5) and *ban*^{1}, *l(3)mbt*^{76} (N=6) brains. N is the number of brain hemispheres quantified. Error bars indicate SEM.

(**c**) Genetic interaction of Ex and *l(3)mbt*^{76}: *GAL4*^{C855a}, *UAS-Ex, l(3)mbt*^{76}/+ control brains, *UAS-Ex, l(3)mbt*^{76} mutant brains and *GAL4*^{C855a}, *UAS-Ex, l(3)mbt*^{76} rescued brains stained for Actin, Deadpan and Prospero (Pros). Scale bars represent 50 μm.

(**d**) Quantification of optic lobe neuroepithelial (NE) volume of *GAL4*^{C855a}, *UAS-Ex, l(3)mbt*^{76}/+ control brains (N=5), *UAS-Ex, l(3)mbt*^{76} mutant brains (N=6) and *GAL4*^{C855a}, *UAS-Ex, l(3)mbt*^{76} rescued brains (N=5). N is the number of brain hemispheres quantified. Error bars indicate SEM.

(**e**) Genetic interaction of *l(3)mbt*^{E2} and *yki*^{B5}: *l(3)mbt*^{E2} single mutant brain and *yki*^{B5}/+; *l(3)mbt*^{E2} double mutant brain stained for Miranda, E-Cadherin and Prospero. Double mutants show suppression of *l(3)mbt*^{E2} phenotype by halving Yki levels (see also Supplementary Fig. S4 b-d for further double mutant brains as well as quantification). Scale bars represent 50 μm.

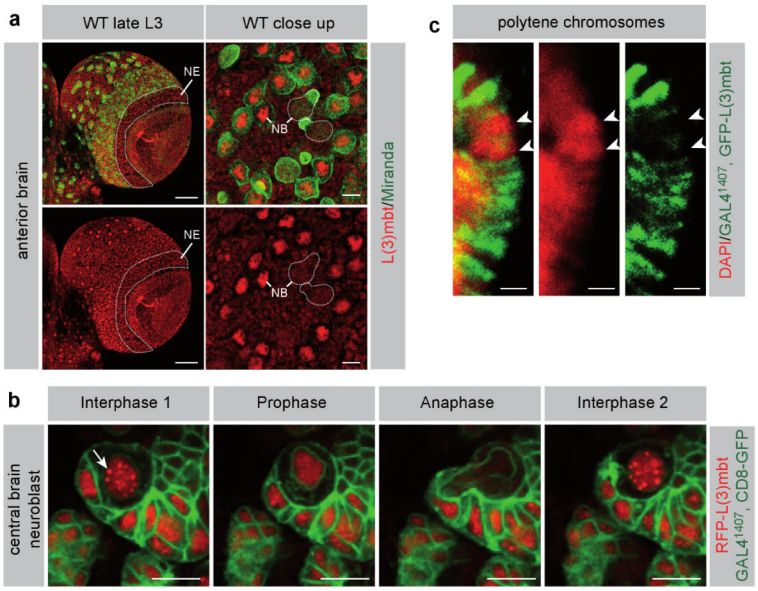

Figure 5. L(3)mbt localizes to the nucleus

(**a**) Larval brain (anterior) stained for L(3)mbt and Miranda. Overview and close up on central brain neuroblasts (NB, outlined) in inter- and anaphase are shown. Note dispersion of L(3)mbt in mitotic NBs. Scale bars represent 50 μm in overview and 10 μm in close up (panels). (Neuroepithelium = NE, outlined in overview)

(**b**) Stills of time lapse imaging of mitotic central brain NB expressing *GAL4*^{1407}*, CD8-GFP* and *RFP-L(3)mbt*. Note that *RFP-L(3)mbt* is reduced and dispersed in the cytoplasm during mitosis. Arrow points to *RFP-L(3)mbt* dots in interphase nuclei. Scale bars represent 10 μm.

(**c**) Close up of polytene chromosome expressing *GAL4*^{1407}*, GFP-L(3)mbt* and stained for DAPI. Arrow heads point to DAPI rich bands at which *GFP-L(3)mbt* is absent. Scale bars represent 1 μm. (See also Supplementary Fig. S5.)

Europe PMC Funders Author Manuscripts

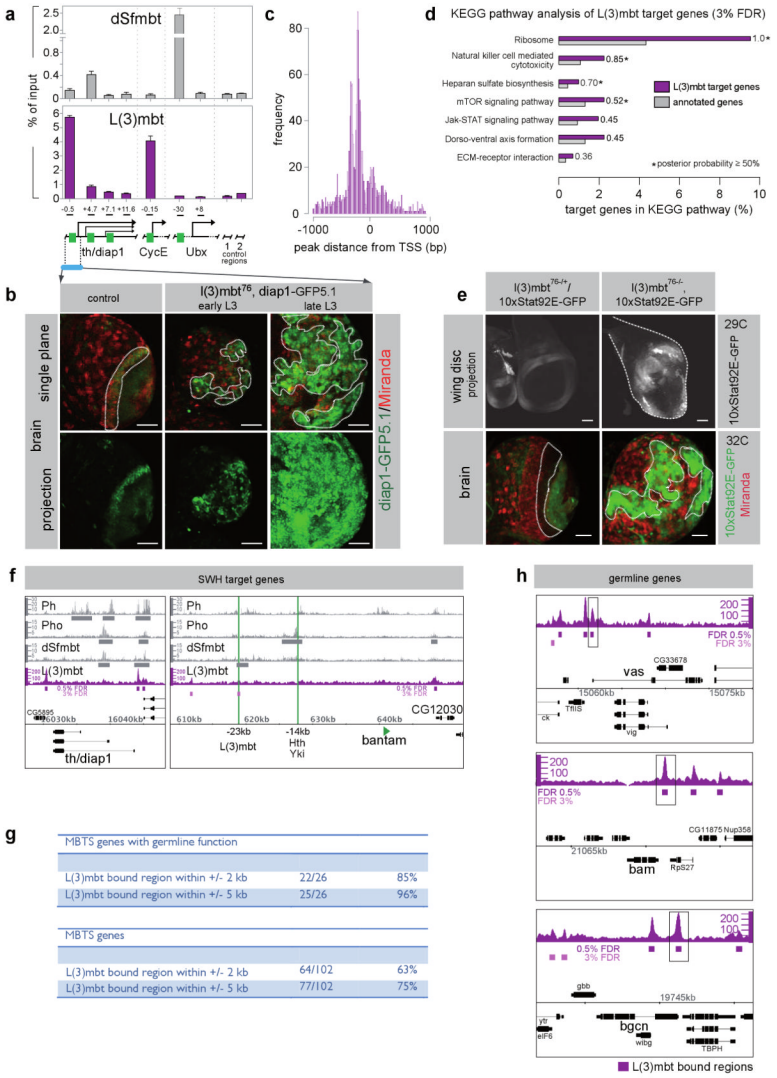

Figure 6. L(3)mbt binds at the TSS and regulates SWH target genes and Jak/STAT pathway activity

(**a**) ChIP analysis at the *th/diap1, CycE, Ubx* and control loci in WT brain and imaginal disc tissues performed with antibodies against dSfmbt and L(3)mbt. ChIP signals at PREs (green boxes) and other regions are presented as percentage of input chromatin (distances from transcription start site (TSS) indicated in kb). Error bars correspond to standard deviation of three ChIP experiments.

(**b**) *diap1-GFP5.1* (including the first TSS of *diap1*) expressed in control and *l(3)mbt*^{76} mutant brains stained for Miranda (single plane in top panels, maximum intensity projections in bottom panels). Scale bars represent 50 μm.

(**c**) Histogram of L(3)mbt binding frequency relative to the closest TSS.

(**d**) KEGG pathway analysis of L(3)mbt target genes (3% FDR). Purple bars represent the observed percentage of target genes in a particular KEGG pathway. Grey bars represent the percentage expected on the basis of all annotated genes. The significance (posterior probability) of this enrichment is based on a Bayesian model-based gene set analysis (MGSA) [48].

(**e**) *10xStat92E-GFP* expressed in wing discs (top panels, maximum intensity projections) and brains (bottom panels, single planes) of *l(3)mbt*^{76}/+ control and *l(3)mbt*^{76} mutant larvae stained for Miranda (bottom panels only). Scale bars represent 50 μm.
(**f**) ChIP-Seq tracks for L(3)mbt (purple) and ChIP-chip tracks for the PcG proteins Ph, Pho and dSfmbt (grey) at the *th/diap1* and *bantam* loci. Purple and grey boxes represent bound regions. For L(3)mbt bound regions at 0.5% and 3% FDR are indicated. Annotated genes and genome coordinate positions correspond to the *Drosophila melanogaster* BDGP Release 5 (UCSC dm3) assembly. Green lines indicate L(3)mbt low occupancy peak at −23kb, and Hth and Yki binding site at −14kb [32] relative to the *bantam* miRNA.
(**g**) Overlap of genes specifically deregulated in *l(3)mbt* mutants [36] (also called MBT signature (MBTS) genes) with genes bound within +/− 2 kb and +/− 5 kb by L(3)mbt. The number of L(3)mbt bound genes versus total number of genes in each category as well as corresponding percentages are shown.
(**h**) ChIP-Seq tracks for L(3)mbt (purple) at germline genes *vas, bam* and *bgcn*. Rectangles outline L(3)mbt binding sites at the TSS. Boxes indicate L(3)mbt bound regions at 0.5% and 3% FDR.

Europe PMC Funders Author Manuscripts

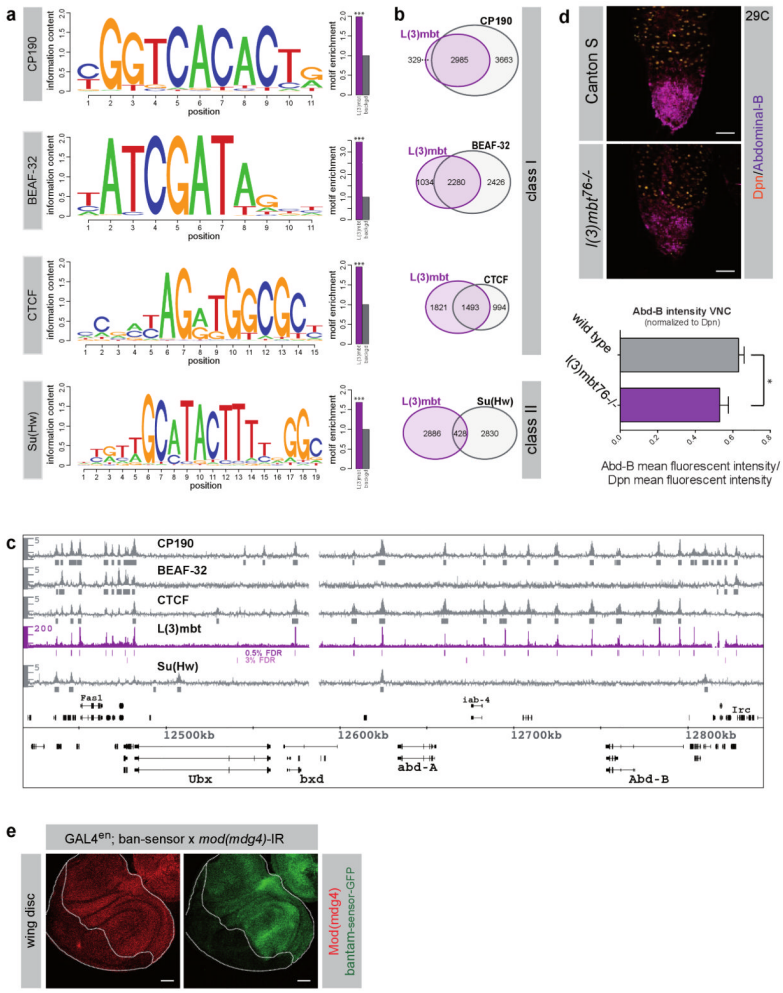

Figure 7. L(3)mbt binds at insulator-bound regulatory domains and influences Abd-B expression

(**a**) *De novo* identified sequence motifs significantly enriched in L(3)mbt bound regions (0.5% FDR) correspond to motifs for the insulator-associated proteins CP190, BEAF-32, CTCF and Su(Hw) [51,52]. Discovered motifs are depicted as sequence logos generated from a position weight matrix (PWM). Histograms show motif enrichment in L(3)mbt bound regions, computed as the ratio of the PWM match frequency in the dataset (purple) and the background (grey) frequency (significance of the enrichment is assessed using Fisher's exact test, ***P<0.001).

(**b**) Venn diagrams showing the overlap of regions bound by L(3)mbt (0.5% FDR, purple) and regions bound by insulator-associated proteins (grey) CP190, BEAF-32 and CTCF (class I insulator proteins), and Su(Hw) (class II insulator protein) [51].

(**c**) ChIP-Seq tracks for L(3)mbt (purple) and ChIP-chip tracks for insulator-associated proteins (grey) CP190, BEAF-32, CTCF and Su(Hw) [51] at the Bithorax complex (BXC) locus. Purple and grey boxes represent bound regions. For L(3)mbt bound regions at 0.5% and 3% FDR are indicated. Annotated genes and genome coordinate positions correspond to the *D. melanogaster* R5/dm3 assembly. (See also Figure S7)

(**d**) Ventral nerve cord (VNC) of control (Canton S) and *l(3)mbt*$^{76-/-}$ mutant brains stained for Deadpan (Dpn) and Abdominal-B (Abd-B). Scale bars represent 50 μm. Graph shows quantification of the Abd-B mean fluorescence intensity normalized to Dpn in control (N=4)

Europe PMC Funders Author Manuscripts

and *l(3)mbt*^{76} (N=6) animals. Error bars represent SEM, p-value (one-tailed) = 0.041 (N is the number of VNCs quantified).
(**e**) Wing disc expressing *GAL4*^{en}; *bantam-sensor-GFP*; *UAS-mod(mdg4)*-IR and stained for Mod(mdg4). Scale bars represent 50 μm.

Europe PMC Funders Author Manuscripts